coatings

MDPI

Article

Synthesis of $CaCO_3$-Based Hyperdispersants and Their Application in Aqueous Coatings

Jue Bai [1,*] and Yu Li [2]

[1] College of Furnishings and Industrial Design, Nanjing Forestry University, Nanjing 210037, China
[2] College of Chemical Engineering, Nanjing Forestry University, Nanjing 210037, China
* Correspondence: nlydh2018@163.com

Abstract: As an essential pigment particle in white water-based coatings, light calcium carbonate ($CaCO_3$) is difficult to disperse in water-based systems. The hard-to-disperse particles agglomerate, causing the viscosity of the coating to rise, which in turn affects the quality of the coating. Therefore, in order to obtain efficient dispersion, the hyperdispersant SSS–MPEGA–DMAEA (SMD) has been prepared in this study using sodium styrene sulfonate (SSS), polyethylene glycol monomethyl ether acrylate (MPEGA), and dimethylaminoethyl acrylate (DMAEA) as monomers through aqueous solution polymerization. Firstly, we utilized the central composite design method to conduct mathematical modeling of the monomer ratios so as to optimize the dispersion performance of the hyperdispersants. Secondly, the structural characteristics and molecular weight distribution of SMD were characterized by ^{1}H NMR spectroscopy and GPC. Then, the effect of SMD on the dispersion of the $CaCO_3$ slurry was investigated through particle size distribution and TEM measurements. Finally, we applied the SMD in aqueous white coatings and tested the surface properties of the paint film by SEM as well as the stability of the paint film. The results showed that SMD can significantly reduce the viscosity and particle size of the $CaCO_3$ slurry. The waterborne coatings prepared by SMD had good storage stability and corrosion resistance, so the materials owned broad application prospects.

Keywords: hyperdispersant; aqueous solution polymerization; $CaCO_3$; aqueous coating

check for updates

Citation: Bai, J.; Li, Y. Synthesis of $CaCO_3$-Based Hyperdispersants and Their Application in Aqueous Coatings. *Coatings* **2023**, *13*, 819. https://doi.org/10.3390/coatings13050819

Academic Editors: Alexandra Muñoz-Bonilla and Alina Vladescu

Received: 18 March 2023
Revised: 20 April 2023
Accepted: 21 April 2023
Published: 23 April 2023

1. Introduction

Light calcium carbonate ($CaCO_3$) is a pigment particle widely used in paper [1], paint [2], rubber [3], adhesives [4] and other industries. It has the advantages of low price, innocuity, good whiteness, etc., so it plays an irreplaceable role in water-based coatings. However, $CaCO_3$ has fine particles, a large specific surface area, and high surface free energy, which can cause delamination or precipitation in aqueous systems, thus affecting product performance [5]. Hyperdispersants, also called polymeric dispersants, are often added to pigment suspensions to effectively inhibit the agglomeration of pigment particles, reduce the viscosity of the system, and form stable and uniform suspensions [6,7]. In addition to the dispersing mechanism of common surfactants, hyperdispersants also have anchoring groups and solventized chains involved in stabilization. There are a large number of anchoring groups in a hyperdispersant molecule, which can be firmly adsorbed on the pigment particles' surfaces through multiple action points and are not easily desorbed [8]. At the same time, due to the larger molecular weight and longer chain length of hyperdispersants, a larger spatial site resistance can be generated when dissolved in the medium, which greatly reduces the probability of mutual collision of the pigment particles themselves [9].

With the rapid development of the coating industry, water-based coatings are gradually taking over the market. The regulations in paint formulations restricting the use of organic solvents have seen the fast development of water-based products [7]. Under the water-based system, pigment particles are more likely to agglomerate, which requires them

to be developed into hyperdispersants with superior performance. On the other hand, most of the hyperdispersants with excellent performance are complicated and mostly synthesized with organic solvents, which may cause some pollution to the environment [10,11]. Therefore, it is a worthy research direction to select suitable monomers so as to synthesize products with excellent performance in a low- or even non-polluting, simple, and low-energy process. Phenyl is an excellent anchoring group and hydrophobic group. Styrene is often shared with maleic anhydride as a raw material for surfactants such as dispersants and water-reducing agents [12,13]. However, the poor compatibility of phenylene with most inorganic materials due to its lack of polar groups limits the application of phenylene in aqueous inorganic material dispersion systems [14]. Therefore, the water-soluble sodium styrene sulfonate (SSS) can be used as a monomer to provide the main anchoring group while providing the phenyl group along with the sulfonic acid group as an effective anchoring group [15–17]. Polyethylene glycol monomethyl ether acrylate (MPEGA), a water-soluble monomer, has a long molecular chain [18]. MPEGA provides hydrophilicity to the copolymer and improves the compatibility with the resin while greatly increasing the spatial site resistance effect [19,20]. Dimethylaminoethyl acrylate (DMAEA) is less hydrophilic. When it provides hydrophobic chain segments, the amine group can provide anchoring groups for the dispersed pigments [21]. The lower initiation temperature of azo diisobutylimidazoline hydrochloride (AIBI) as an initiator makes it less prone to burst polymerization, so it is easier to control the reaction temperature when aqueous polymerization is carried out, resulting in the higher stability of the product properties [22]. Based on these monomers, we would like to develop a hyperdispersant with high dispersion performance, low pollution, low cost, and low dosage, which can make the $CaCO_3$ pigment particles uniformly dispersed in an aqueous system. Additionally, in practical applications, it can improve the stability of calcium carbonate in white coatings and enhance the performance of coatings. In this paper, we innovatively use SSS and DMAEA to solve the solubility problem of monomers in water, possessing effective hydrophobic chain segments and anchoring groups, and the effective spatial site resistance is provided by MPEGA as a solventized chain segment. Aqueous hyperdispersants synthesized by this method are very effective in dispersing $CaCO_3$ particles, which has not been reported in the existing literature and is important for the redevelopment of aqueous hyperdispersants.

In this study, the copolymer SSS–MPEGA–DMAEA has been obtained by aqueous polymerization using SSS, DMAEA and MPEGA as monomers and AIBI as an initiator. After preparing white water-based coatings with acrylic resin as the film-forming substance and $CaCO_3$ as the filler, the stability, water resistance, acid and alkali resistance, as well as other practical application properties of the paint film, were investigated with the addition of the hyperdispersant.

2. Experimental Section

2.1. Materials

During the experiments, the following starting materials were used. Sodium p-styrenesulfonate (SSS, 90%) and azo diisobutyl imidazoline hydrochloride salt (AIBI, 98%) were obtained from Shanghai Macklin Biochemical Co., Ltd. in Shanghai, China. Polyethylene glycol monomethyl ether acrylate (MPEGA, ≥90%) was supplied by Liaoning Kolon Fine Chemical Co., Ltd. in Liaoning, China. Dimethylaminoethyl acrylate (DMAEA, 99%) was bought from Shanghai Aladdin Biochemical Technology Co., Ltd. in Shanghai, China. Light calcium carbonate ($CaCO_3$, 2500 items) was obtained from Shanghai Hover Chemical Co., Ltd. in Shanghai, China. The MixSperse 855 W hyperdispersants (quality score number of 50%) were supplied by Wuxi Mikos New Material Technology Co., Ltd. in Wuxi, China. E504 acrylic resin (40%) was bought from Shenzhen Yoshida Chemical Co., Ltd. in Shenzhen, China. Surfynol DF-110C defoamer (20%) was supplied by Air Products Inc., Ltd. in Arlington, United States. Titanium white (TiO_2, 1250 items) was obtained from Sichuan Long Python Titanium Industry Co., Ltd. in Mianzhu, China. Propylene glycol methyl ether (PGMEA, CP) was obtained from Yong Hua Chemical Technology (Jiangsu) Co., Ltd.

in Changshu, China. Sodium hydroxide (NaOH, AR) and sulfuric acid (H_2SO_4, AR) were bought from Nanjing Chemical Reagent Co., Ltd. in Nanjing, China.

2.2. Synthesis of Copolymer SSS–MPEGA–DMAEA

A certain mass of SSS, MPEGA, and DMAEA was weighed and dissolved in deionized water, and AIBI with a monomer concentration of 8% was added to make the monomer concentration 1 mol/L. The solution was added into a four-necked flask, and nitrogen gas was passed to exhaust the oxygen of the reaction system. The solution was stirred and slowly warmed up to 66 °C for 4.5 h to obtain the hyperdispersant SSS–MPEGA–DMAEA (SMD), and the effective content was adjusted to 50% (mass fraction, same as below). The reaction equation is shown in Figure 1.

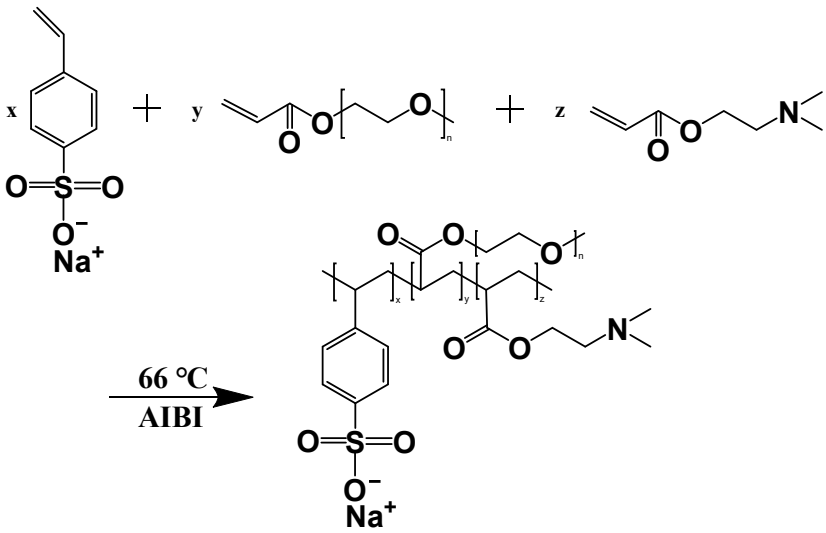

Figure 1. Reaction equation of SSS–MPEGA–DMAEA.

2.3. Formulation of Pigment Pastes and Coatings

The dispersant, $CaCO_3$, and deionized water were mixed in a certain proportion to make a 50% solid content slurry, and the pigment slurry was produced by using an SF-type intelligent dispersion sand mill (Weite, Shanghai, China) at 2000 r/min for 20 min.

The film-forming substances, pigments, solvents and additives were mixed in a certain ratio and dispersed at 1500 r/min for 30 min under the action of a dispersion sander to prepare water-based coatings. The reference formula is shown in Table 1.

Table 1. Proportioning of coatings.

Coating Composition	Acrylic Resin	Dispersants	Defoamer	$CaCO_3$	TiO_2	PGMEA	Deionized Water
Percentage of components (%)	65	0.5	0.03	15.5	8	4	6.97
Dosage (g)	32.5	0.25	0.015	7.75	4	2	3.485

2.4. Central Composite Design of Hyperdispersant Monomer Ratios

Central composite design (CCD) is a response surface methodology (RSM) and a chemometric tool for building quadratic models to determine nominal values (maxima or minima) of factors for modeling processes from two or more factors [23]. The viscosity and stability of the slurry with a $CaCO_3$ mass fraction of 50% were investigated, and the three monomer ratios of SSS, MPEGA, and DMAEA were used as optimization factors to design the experiments by the central composite design method. The optimal group in the pre-experiment was set in the center, i.e., the dosage of SSS was 2 mol, the dosage of MPEGA was 0.3 mol, and the dosage of DMAEA was 1.5 mol. The experimental factors and levels are shown in Table 2.

Table 2. Factors and levels of central composite design.

Level	Factors		
	Amount of SSS (X_1, mol)	**Amount of MPEGA (X_2, mol)**	**Amount of DMAEA (X_3, mol)**
−1.68	0.32	0.13	0.66
−1	1	0.2	1
0	2	0.3	1.5
1	3	0.4	2
1.68	3.68	0.47	2.34

2.5. Testing and Characterization

2.5.1. Characterization of the Hyperdispersant SSS–MPEGA–DMAEA

Nuclear magnetic resonance hydrophobic (^{1}H NMR) analysis was performed using a 400 MHz full digital superconductivity NMR spectrometer (Bruker, Ettlingen, Germany). The tests were conducted with tetramethylsilane (TMS) as the internal standard and heavy water (D_2O) as the solvent

The molecular weight was measured using a Waters GPC comprising a Waters 1525 HPLC pump, a Waters 2414 refractive index detector, and a Waters 717 autosampler (Tosoh, Tokyo, Japan). The eluent was water at a flow rate of 1.0 mL/min, and the temperature was set as 35 °C.

2.5.2. Hyperdispersant Dispersion Performance Test

The viscosity of the $CaCO_3$ dispersion slurry was determined by an NDJ-5S rotational viscometer (Pingxuan, Shanghai, China), in which the hyperdispersants accounted for 0.3%, 0.4%, 0.5%, 0.6%, and 0.7% of the calcium carbonate content, respectively.

The particle size of the $CaCO_3$ slurry was diluted 100 times and run through a Malvern Zeta Sizer instrument (Malvern Instruments, Malvern, UK).

The $CaCO_3$ dispersion slurry was prepared after obtaining the optimum amount of dispersant, and the viscosity variation with temperature was tested by a Physica MCR 301 rheology analyzer (Anton Paar, Graz, Austria).

The $CaCO_3$ slurry with the optimum hyperdispersant content was diluted 100 times, and the morphology of $CaCO_3$ was observed in a JEM-2100 UH R high-resolution transmission electron microscope (TEM) (JEOL, Tokyo, Japan).

2.5.3. Paint Suspension Rate Stability Test

The prepared coatings were packed into air-tight containers and stored at room temperature. The suspension rate w (%) of the active ingredient in the water-based paint was measured under the standard GB/T 14825-2006, as shown in Equation (1).

$$w = \frac{M - m}{M} \times \frac{10}{9} \times 100\% \tag{1}$$

where: M is the mass of the active ingredient in the formulated water-based paint in grams (g); m is the active ingredient left in the bottom 1/10 of the water-based paint in grams (g), and 10/9 is the conversion factor.

2.5.4. Coating Viscosity Change Test

The prepared paint was loaded into a well-gas-tight container, and the container was opened and stirred with a glass rod for 30 s every week to test and record the change in the viscosity of the paint. The change of viscosity with time is examined as the rate of change R [24]. The initial viscosity is V_0, the changed viscosity is V_t, and the rate of change of viscosity with time is R, as shown in Equation (2).

$$R = \frac{V_t - V_0}{V_0} \times 100\% \tag{2}$$

where V_0 is the initial paint viscosity in mPa·s; V_t is the paint viscosity over time in mPa·s.

2.5.5. Water Resistance Test of Paint Film

The prepared paint was applied to the test plate and then cured and dried for 24 h. A total of 2/3 of the length of the test plate was submerged in deionized water and placed at a constant temperature of 25 °C. The blistering, rusting, peeling, and chalking of the test plate were observed and recorded. The judging standard adopted was GB-T 1766-2008, which is a rating method of color and varnish coating aging.

2.5.6. Acid Resistance Test of Paint Film

The prepared paint was applied to the test plate and then dried and cured for 24 h. A total of 2/3 of the length of the test plate was submerged in a 5% concentration of sulfuric acid solution and placed at a constant temperature of 25 °C. The blistering, rusting, flaking, chalking, and other phenomena of the test plate were observed and recorded. The judgment standard adopted was GB-T 1766-2008, which is a rating method of color and varnish coating aging.

2.5.7. Alkali Resistance Test of Paint Film

The prepared paint was applied to the test plate and then dried and cured for 24 h. A total of 2/3 of the test plate was submerged in a 5% concentration of sodium hydroxide solution and placed at a constant temperature of 25 °C. The blistering, rusting, flaking, chalking, and other phenomena of the test plate were observed and recorded. The judgment standard adopted was GB-T 1766-2008, which is a rating method of color and varnish coating aging.

2.5.8. Environmental Scanning Electron Microscope Test of Paint Film

After mechanical stirring, the same mass of paint was applied uniformly to the test plate. The test panels were allowed to cure at room temperature for 24 h, and the surface properties of the paint films were observed using an FEI Quanta 200 environmental scanning electron microscope (SEM) (FEI, Hillsboro, OR, USA) after sampling.

3. Results and Discussion

3.1. Central Composite Design

The results are shown in Table 3 after examining each level factor of monomer dosage by central composite design with the viscosity of the dispersed slurry as the index.

Table 3. Experimental results of central composite design.

Serial Number	X_1 (mol)	X_2 (mol)	X_3 (mol)	Y (mPa·s)
1	3.68	0.30	1.50	102
2	2.00	0.30	1.50	116
3	2.00	0.30	1.50	104
4	3.00	0.40	1.00	115
5	2.00	0.30	0.66	101
6	1.00	0.20	2.00	424
7	3.00	0.40	2.00	139
8	1.00	0.20	1.00	153
9	2.00	0.30	1.50	104
10	1.00	0.40	2.00	529
11	3.00	0.20	1.00	75
12	3.00	0.20	2.00	77
13	2.00	0.30	1.50	105
14	2.00	0.47	1.50	169
15	2.00	0.30	2.34	130
16	2.00	0.13	1.50	104

Table 3. *Cont.*

Serial Number	X_1 (mol)	X_2 (mol)	X_3 (mol)	Y (mPa·s)
17	0.32	0.30	1.50	805
18	2.00	0.30	1.50	109
19	1.00	0.40	1.00	362

Note: X_1 is the amount of SSS, X_2 is the amount of MPEGA, X_3 is the amount of DMAEA, and Y is the viscosity of the slurry.

The linear regression equation, response surface, and contours yield the regression equation presented in Equation (3).

$$Y = 119.96 - 167.69X_1 + 35.23X_2 + 34.27X_3 - 32.15X_1X_2 - 57.15X_1X_3 - 15.95X_2X_3 + 115.16{X_1}^2 + 3.08{X_2}^2 - 4.27{X_3}^2 \quad (3)$$

where X_1 is the amount of SSS in mol, X_2 is the amount of MPEGA in mol, X_3 is the amount of DMAEA in mol, and Y is the viscosity of the slurry in mPa·s.

The equation's goodness of fit R^2 = 0.9587 (the R value is the correlation coefficient). A closer R^2 value to 1 indicates an improved fit for the multiple linear regression equation, enhancing the congruence between this regression equation and the actual data. The central composite design's optimal values are X_1 = 2.56 mol, X_2 = 0.23 mol, and X_3 = 1.44 mol.

Table 4 offers a statistical analysis of the experimental outcomes. The p-values of X_1, X_2, and X_3 within the independent variables, X_1X_3 in the interaction term, and ${X_1}^2$ in the quadratic term are lower than the significant level α = 0.1, signifying the substantial effect of each of these items. The p-values of X_1X_2 and X_2X_3 in the interaction term and ${X_2}^2$ and ${X_3}^2$ in the secondary term exceed the significant level α = 0.1, suggesting an insignificant effect of this item.

Table 4. Statistical analysis of experimental results.

Parameters	Coefficients and p-Values of the Multiple Linear Regression Equation		
Independent variables	X_1 −89.16 (<0.0001)	X_2 45.38 (0.0434)	X_3 16.27 (0.0483)
Interaction items	X_1X_2 −65.70 (0.1354)	X_1X_3 −23.45 (0.0172)	X_2X_3 1.70 (0.4369)
Secondary items	${X_1}^2$ 59.70 (<0.0001)	${X_2}^2$ 28.16 (0.8418)	${X_3}^2$ 12.25 (0.7824)

Note: The values in parentheses are p-values; the smaller the value, the more significant the effect of the factor on the indexes examined.

According to the p-value analysis, the fitted equation can be simplified to Equation (4) by deleting the non-significant effect term.

$$Y = 119.96 - 167.69X_1 + 35.23X_2 + 34.27X_3 - 57.15X_1X_3 + 115.16{X_1}^2 \quad (4)$$

where X_1 is the amount of SSS in mol, X_2 is the amount of MPEGA in mol, X_3 is the amount of DMAEA in mol, and Y is the viscosity of the slurry in mPa·s.

Figure 2 indicates the curves of the $CaCO_3$ slurry's viscosity in relation to each factor's variation. With the escalation of DMAEA in the reaction monomer, the viscosity of the suspension slurry initially declines and subsequently increases, implying that dispersion performance first improves and then deteriorates. This is due to DMAEA providing not only the primary hydrophobic group but also a potent anchoring group in the form of an amine group. This group forms strong bonds with the pigment particles, is difficult to desorb, and has a benign effect on the stability of the suspension slurry. However, an excessive proportion of the anchoring group results in the hyperdispersant's molecular chain adsorbing numerous pigment particles, yielding "bridging" and eventual flocculation and sedimentation. The suspension slurry viscosity initially diminishes and then surges as the MPEGA dosage in the reaction monomer increases, indicating that dispersion performance first strengthens and then weakens. This occurs because the polyether chain in

MPEGA provides significant steric resistance for the hyperdispersant molecules, effectively preventing the adsorbed pigment particles from aggregating, sedimenting, and causing flocculation. As MPEGA quantity rises, the spatial site resistance effect will be strengthened. However, if the polymer molecular chains are too long, they will also adsorb multiple pigment particles, leading to agglomerative settling and eventually leading to poor slurry stability. The viscosity of suspension slurry exhibits a decline, followed by an increase, as the concentration of SSS in the reaction monomer rises, indicating an enhancement, then deterioration, in dispersal performance. Owing to the phenyl group of SSS acting as an excellent anchoring group, the pigment particles are wrapped by the phenyl group, promoting the stability of the suspension slurry. However, excessive SSS can result in a "bridging" phenomena, ultimately raising slurry viscosity.

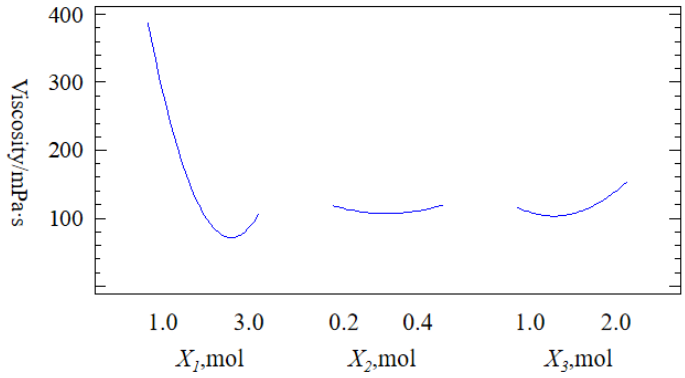

Figure 2. Effect of various factors on the viscosity of $CaCO_3$ paste.

The effects of SSS, MPEGA, and DMAEA on the dispersion of calcium carbonate by SMD hyperdispersants are displayed in Figures 3–5. From the three-dimensional plots and contour plots, the minimum $CaCO_3$ slurry viscosity occurs at 2.5~2.6 mol for SSS, 0.2~0.3 mol for MPEGA, and 1.4~1.5 mol for DMAEA.

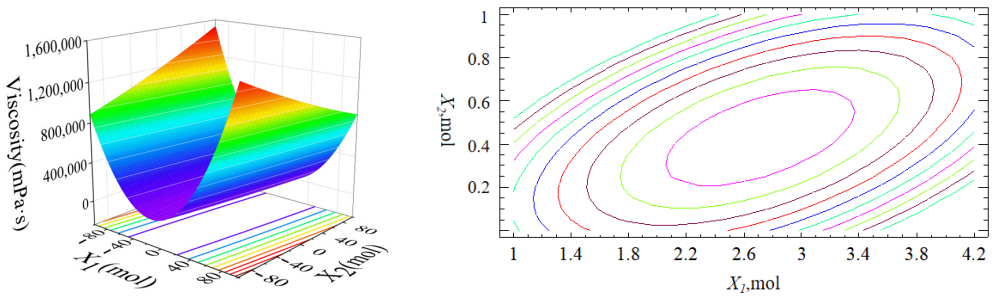

Figure 3. Three-dimensional and contour plots of the effect of SSS dosage and MPEGA dosage on the viscosity of calcium carbonate slurry.

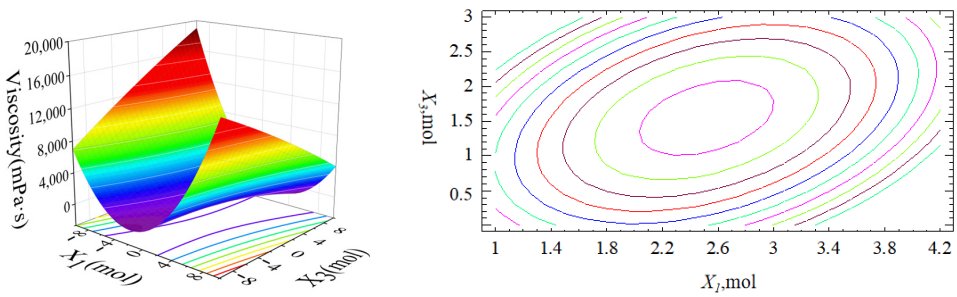

Figure 4. Three-dimensional and contour plots of the effect of SSS dosage and DMAEA dosage on the viscosity of calcium carbonate slurry.

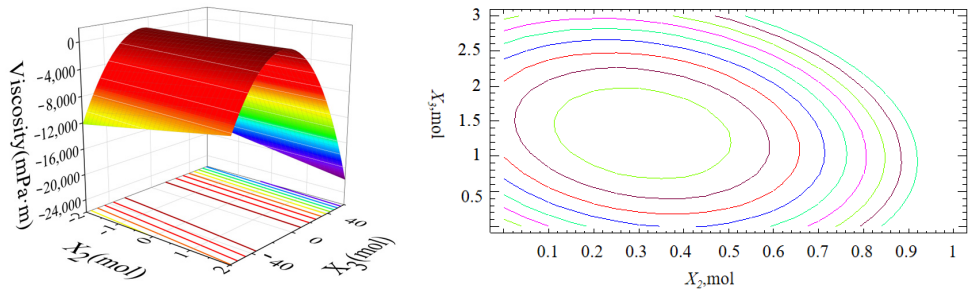

Figure 5. Three-dimensional and contour plots of the effect of MPEGA dosage and DMAEA dosage on the viscosity of calcium carbonate slurry.

The prediction function of the fitted equation at the optimal process point for slurry viscosity theory was verified by repeating the experiment three times and preparing $CaCO_3$ separately to determine the viscosity, and the results are shown in Table 5. The performance of the hyperdispersant SMD, prepared by the optimized formulation of the central composite design method, is better, with a smaller deviation of the slurry viscosity from the predicted value. This indicates that the prediction of the multiple linear regression equation is good and the confidence is high. Consequently, the central composite design method exhibits a more pronounced effect on optimizing the formulation of the hyperdispersant SMD, and the resulting copolymer demonstrates exceptional performance.

Table 5. Predicted and experimental values for the viscosity of light calcium carbonate slurry.

Category	Slurry Viscosity (mPa·s)					
	Experimental Value			Average Value	Predicted Value	Deviation
$CaCO_3$	55	67	62	61.3	60	1.3

3.2. Characterization of Hyperdispersant SSS–MPEGA–DMAEA

3.2.1. Nuclear Magnetic Resonance Hydrogen Spectroscopy (^{1}H NMR) Analysis

The optimal hyperdispersant ratio is obtained as n(SSS): n(MPEGA): n (DMAEA) = 9:1:5.4 by mathematical modeling through the central composite design method to optimize the process conditions. The terpolymer SSS–MPEGA–DMAEA, synthesized via aqueous solution polymerization, exhibits the NMR hydrogen spectrum illustrated in Figure 6.

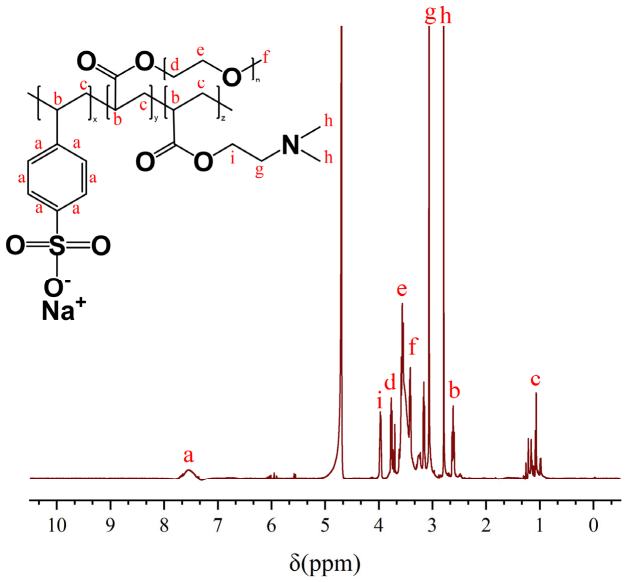

Figure 6. ^{1}H NMR spectra of SSS–MPEGA–DMAEA.

From the figure, the D_2O solvent peak is obtained at δ = 4.7 ppm. The proton peak at δ = 7.3~7.7 ppm corresponds to the chemical shift of the hydrogen on the benzene ring (a). The proton peak at δ = 2.5~2.65 ppm is the chemical shift of the hydrogen on the hypomethyl group, formed due to polymerization by opening the double bond with each monomer (b). The proton peak at δ = 0.9~1.3 ppm indicates the chemical shift of hydrogen on methylene, formed on each monomer due to double bond opening and due to polymerization (c). The proton peak at δ = 3.7~3.85 ppm represents the chemical shift of the hydrogen on the methylene group, which is attached to the ester group (d). The proton peak at δ = 3.6 ppm denotes the chemical shift of the hydrogen on the methylene group linked to the ether bond (e). The proton peak at δ = 3.3 ppm exhibits the chemical shift of the hydrogen on the methyl group connected to the ether bond (f). The proton peak at δ = 2.9~3.2 ppm highlights the chemical shift of the hydrogen on the methylene group attached to the tertiary amine group (g). The proton peak at δ = 2.8 ppm is the chemical shift of the methyl hydrogen on the tertiary amine group (h). The proton peak at δ = 3.9 ppm corresponds to the chemical shift of the hydrogen on the methylene group (i). Consequently, the resulting polymer is a terpolymer of SSS, MPEGA, and DMAEA, and the resultant copolymer is the target product.

3.2.2. Gel Permeation Chromatography (GPC) Analysis

The GPC test results are shown in Figure 7. In Figure 7a, dwt/d signifies the molecular weight differential distribution, while Cumulative indicates the cumulative distribution of the molecular weight. Figure 7b shows the relative molecular weight distribution of the hyperdispersant SMD. The polymer prepared at the optimum point, ascertained by the central composite design method, exhibited a standard distribution of relative molecular masses. The relative molecular mass at the highest peak (M_p) was 12,445, the numerical mean molecular weight (M_n) was 5531, and the heavy mean molecular weight (M_w) was 12,442. If the relative molecular mass distribution is excessively broad, a grading phenomenon will occur. This means that a portion of the polymer is free in the water that is unable to bind closely to the pigment particles or is prone to desorption due to excessively low or high relative molecular mass. Polymers with low-molecular-weight and narrow-molecular-weight distributions are more efficacious as dispersants than those with wide-molecular-weight distributions [7]. This results in an enhanced dispersion of the hyperdispersants SMD with relative molecular masses around 12,400.

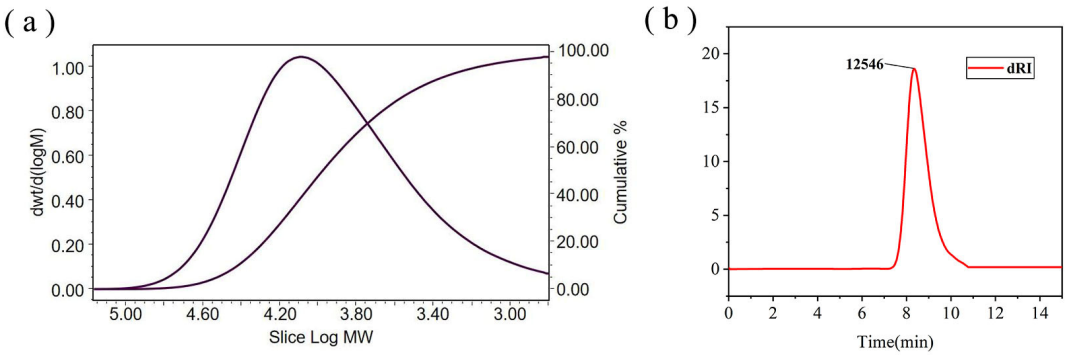

Figure 7. Relative molecular mass distribution of hyperdispersant SSS–MPEGA–DMAEA. (**a**) The molecular weight differential distribution and the cumulative distribution of the molecular weight; (**b**) The distribution of average molecular weight.

3.2.3. Particle Size Analysis

Dynamic light scattering (DLS) measurements were conducted on $CaCO_3$ samples dispersed in water in suspension to determine the particle size distribution of $CaCO_3$ in aqueous media [25]. Standard $CaCO_3$ slurries with identical solid contents were prepared with the SSS–MPEGA–DMAEA hyperdispersant and MixSperse 855 W hyperdispersant, respectively, and subsequently diluted 100 times to test the particle size. From Figure 8, the

particle sizes of $CaCO_3$ slurry produced by the MixSperse 855 W and SSS–MPEGA–DMAEA hyperdispersants both exhibited normal distributions. The average particle size of $CaCO_3$ slurry made by 855 W was 1472 nm, whereas that produced by SSS–MPEGA–DMAEA was 1119 nm. The SSS–MPEGA–DMAEA hyperdispersant prevented the agglomeration of pigment particles and reduced the particle size effectively, surpassing the performance of some commercially available dispersants.

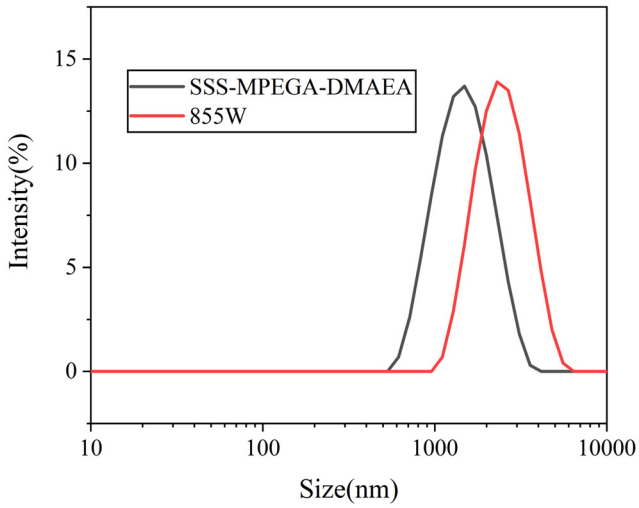

Figure 8. Particle size distribution of $CaCO_3$ paste.

3.3. Optimal Amount of Hyperdispersant

Figure 9 displays the viscosity curves of light calcium carbonate (2500 mesh) with 50% solid content and different quantities of homemade hyperdispersant (effective content). Each viscosity value in the graph is an average of three measurements, and the error bars represent the standard deviation of the three measurements. The pigment paste's viscosity shows a trend of decreasing and then increasing with the rise in hyperdispersant quantity. This occurs because when the amount of hyperdispersant is minimal, some pigment particles cannot be wrapped by the hyperdispersant molecules and are prone to agglomeration and sedimentation. When the amount of hyperdispersant is excessive, multiple polymer molecular chains are combined with the pigment particles, and the long chains are entangled with each other, causing the phenomenon of "bridging", resulting in the agglomeration and settling of pigment particles.

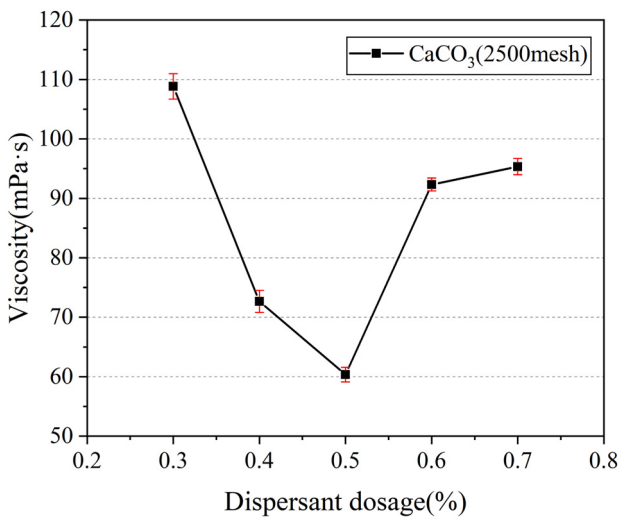

Figure 9. Effect of dispersant dosage on paste viscosity.

Figure 10 illustrates the comparison of the average particle size of $CaCO_3$ slurry for different dispersant contents. Evidently, when the dispersant concentration is 0.5%, the slurry exhibits the smallest average particle size, indicating optimal dispersion efficacy. Insufficient dispersant concentrations lead to ineffective dispersion, resulting in $CaCO_3$ particle agglomeration and larger molecular particle sizes within the slurry. Conversely, excessive dispersant concentrations cause particle agglomeration and increased average particle sizes. The optimal hyperdispersant quantity is related to the paste's solid content and the pigment's particle size and specific gravity. The higher the solid content, the more difficult it is to disperse the color paste, and the best amount of dispersant will be increased. The smaller the particle size of the pigment, the larger the surface energy of the particles, and the easier they agglomerate, resulting in more difficulty in dispersing the color paste and an increase in the best dispersant dosage. The larger the specific gravity of inorganic pigments, the smaller the volume of pigments in the same solid content of the color paste, and the easier it will be to disperse; as a result, the best dispersant dosage will be reduced.

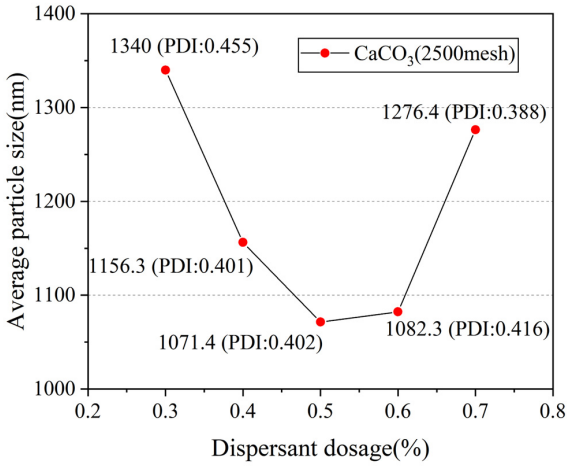

Figure 10. Effect of dispersant dosage on average particle size of slurry.

The variation of slurry viscosity with shear rate as tested by the rheology analyzer is shown in Figure 11. As far as the effect of temperature on viscosity is concerned, the viscosity generally tends to decrease as the temperature increases. With the increase in temperature, the intermolecular attractive force acting between pigment particles and water molecules reduces, which, in turn, reduces viscosity values [26]. Additionally, it can be observed from the graph that the viscosity of the slurry at different temperatures is relatively close. Therefore, the stability of the slurry is not much affected by the temperature under normal room temperature conditions.

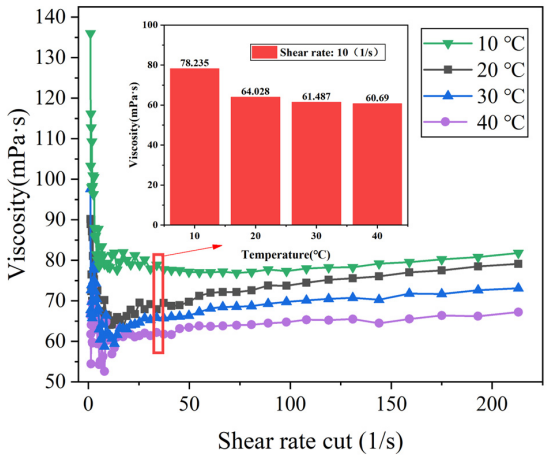

Figure 11. Effect of temperature on the viscosity of calcium $CaCO_3$.

Figure 12 presents the TEM image of the $CaCO_3$ slurry after adding the optimal dispersant amount at a 100-fold magnification. Figure 12A shows the dispersion of the slurry, revealing that the pigment particles under the aqueous solution dispersion system of the SMD copolymer did not form larger particles, although there was agglomeration. Figure 12B depicts the SMD copolymer, which can be seen to have adsorbed on the surface of calcium carbonate particles, producing a dispersion effect. The surface volume ratio or surface energy of $CaCO_3$ increases when a dispersant is attached to its surface, which is why its particles tend to agglomerate very little [27].

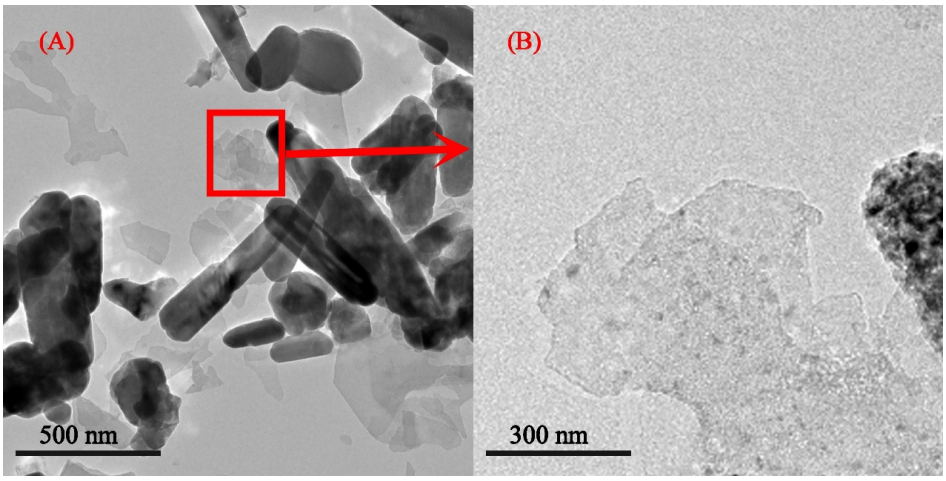

Figure 12. TEM images of pastes prepared with SMD. (**A**) TEM images of 500 nm; (**B**) TEM images of 300 nm.

A microscopic explanation of the dispersant dispersion mechanism is illustrated in Figure 13. The anchoring groups provided by SSS and DMAEA enable the hyperdispersants to be firmly adsorbed on the pigment particle surface. The ultra-long solventized chains of DMAEA and MPEGA provide sufficient spatial site resistance to stabilize the system and prevent the suspended particles from agglomerating and settling. At the same time, the electrostatic repulsion generated by the charges formed on the particle surface by SMD will also prevent the agglomeration of pigment particles.

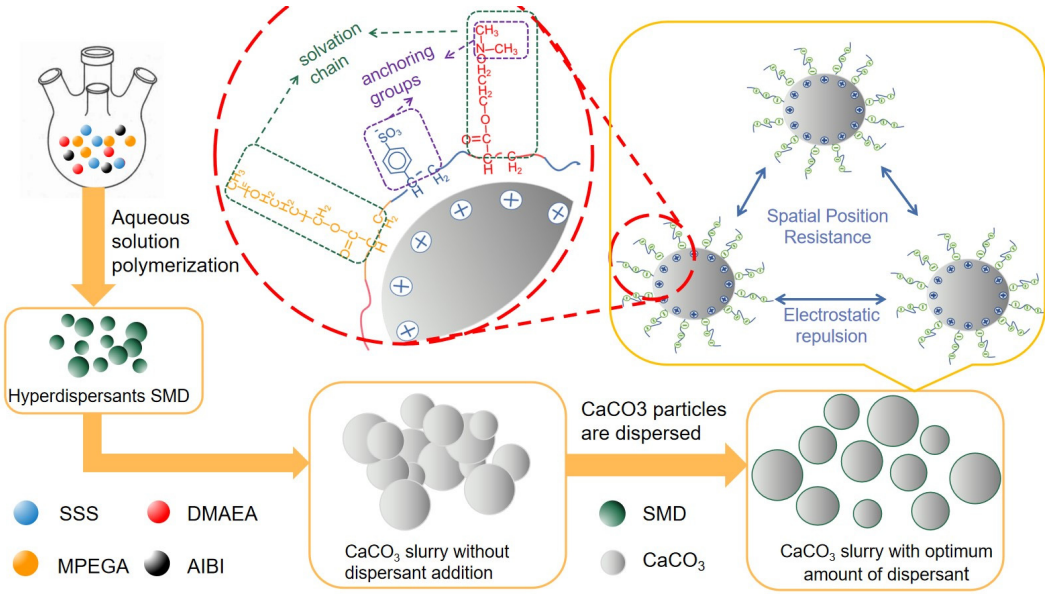

Figure 13. The process of hyperdispersant SMD dispersion of $CaCO_3$.

3.4. Coating Performance Characterization

3.4.1. Stability of Coating Suspension Rate

During storage of the paint, inevitable physical and chemical alterations transpire, potentially impacting the product's regular utilization. Therefore, it is also essential to evaluate the storage stability of coatings. Hyperdispersants not only act on the surface of pigment particles but also function as surfactants on the surface of emulsions to prevent the coalescence of emulsion particles. Figure 14 shows the effect of two dispersants on the suspension rate of active ingredients in aqueous coatings.

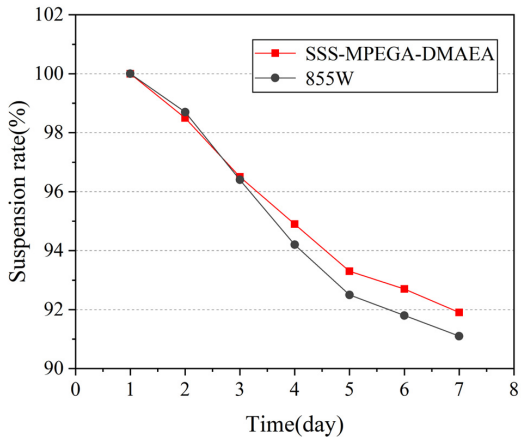

Figure 14. Effect of storage time on paint suspension rate.

As storage time increased, the suspension rate diminished, and the rate of change progressively decreased. However, a noticeable disparity in suspension rate variations existed when employing different hyperdispersants as additives. From the first day to the third day, the suspension rate of the 855 W hyperdispersant group was slightly higher than that of the homemade dispersant group. However, on the fourth day, the suspension rate of the homemade dispersant group started to be higher than that of the 855 W hyperdispersant group, with a discernible difference emerging over time. This indicates that the SSS–MPEGA–DMAEA hyperdispersant exhibits excellent storage stability.

3.4.2. Coating Viscosity Stability

After the production of paint, transportation and storage necessitate a specific duration, during which gravity-induced pigment and filler sedimentation cause viscosity and performance alterations. In actual usage, they will be stirred well before being put into actual use. Therefore, whether they can return to their initial state after stirring is also one of the issues to be considered when redeveloping the product. Figure 15 displays the viscosity stability curve of water-based coatings prepared by two hyperdispersants.

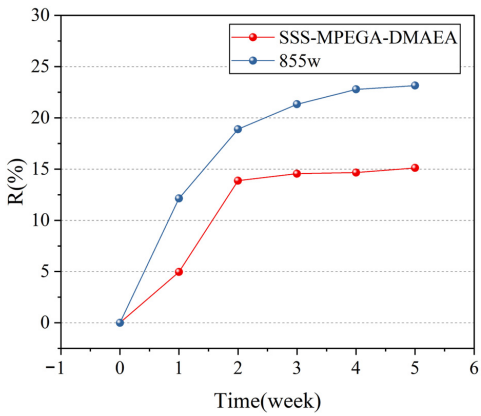

Figure 15. Effect of storage time on viscosity change rate.

The viscosity of the paint after simple mixing became larger with an increase in storage time, indicating that the pigment particles did settle. The viscosity change rate showed a trend of being fast and then gradually stabilizing, and the change trend slowed down after the second week. The rate of change of the homemade hyperdispersant is relatively more stable compared with 855 W in practical application.

3.4.3. Water Resistance of Paint Film

The bubbling of the paint film in water with time is displayed in Figure 16a, where the bar graph shows the density change of bubbling, and the dotted line graph signifies the size change of bubbling. The diagram reveals that the coating fabricated using the 855 W dispersant initiated blistering on the fourth day, with noticeable blistering by day six. The self-made dispersant started to blister on the fifth day, with discernible bubbles by day seven. The water resistance of the waterborne coatings prepared by the two hyperdispersants was good after film formation, with the SMD hyperdispersant slightly surpassing that of 855 W.

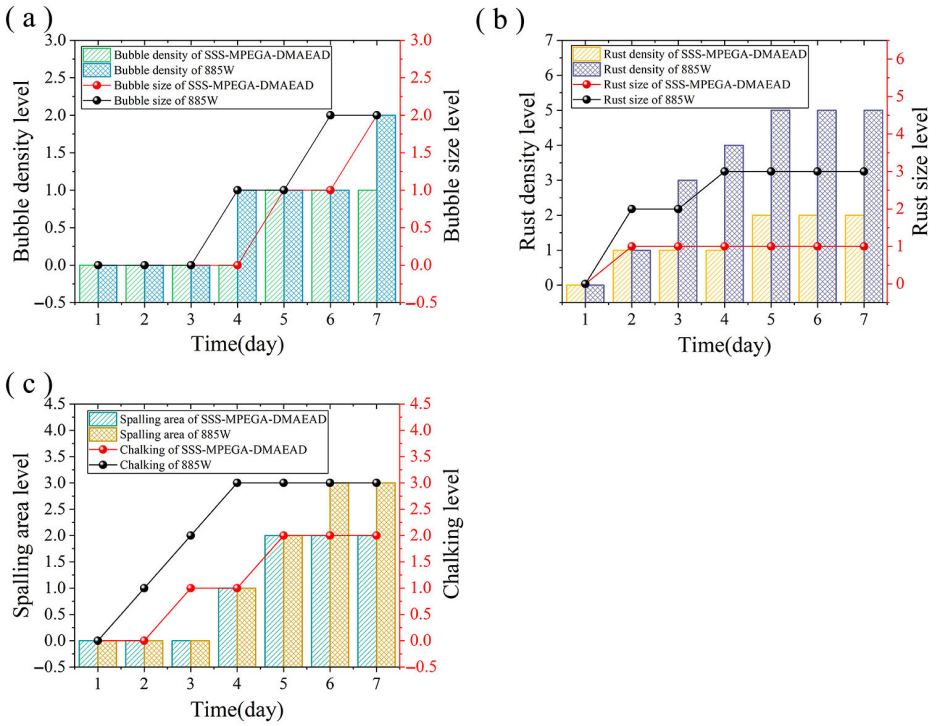

Figure 16. The water resistance of paint film. (**a**) Blistering of the paint film in water; (**b**) Rusting of the paint film in water; (**c**) Flaking of the paint film in water.

Figure 16b portrays the rusting of the paint film in water with time, where the bar graph represents the density change of rusting and the dotted line graph illustrates the size change of rusting. As the graph indicates, rust spots started to appear on the 2nd day after the film formation of both kinds of paint prepared by hyperdispersants. However, the rate of rust spots and the rate of increase in the area of the paint prepared by homemade hyperdispersants were lower than that of 855 W. Oxygen in the air dissolved in water will react with the paint after the film formation, resulting in rust spot emergence. A portion of the homemade hyperdispersant SMD in water will ionize into cations, and the cationic surfactant has a certain anti-corrosion effect.

The peeling and chalking of the paint film in water with time are demonstrated in Figure 16c, with the bar graph depicting the change in the peeling area and the dotted line graph signifying the change in the chalking level. The coating film prepared by both hyperdispersants started to flake off on day 2, although the situation of the experimental group with the homemade hyperdispersant was better than that of the experimental group

with MixSperse 855 W. A minimal quantity of pigment particles emerged on day 4 for the experimental group with the MixSperse 855 W hyperdispersant, while a comparable phenomenon occurred on day five for the homemade hyperdispersant group. These observations are correlated with the extent of foaming and rusting.

From the corrosion of the paint film in water, the homemade hyperdispersant SMD can make the paint film have better water resistance.

3.4.4. Acid Resistance of Paint Film

Figure 17a shows the bubbles of the paint film in 5% sulfuric acid over time, where the bar graph indicates the density change of bubbling and the dotted line graph signifies the size change of bubbling. The bubbles started to appear on the fourth day for the coating prepared by the homemade dispersant, with an increased bubble count on day five. Conversely, the MixSperse 855 W dispersant initiated bubble appearance on the third day, with a higher bubble count on day four. In both experimental groups, larger bubbles surfaced on day three, enlarging with prolonged immersion time due to the enhanced corrosiveness of the potent acid solution compared to deionized water. The paint film will not only react with oxygen but also with hydrogen ions. The strong acid will even react with the test plate through the paint film to produce more substantial and more abundant bubbles.

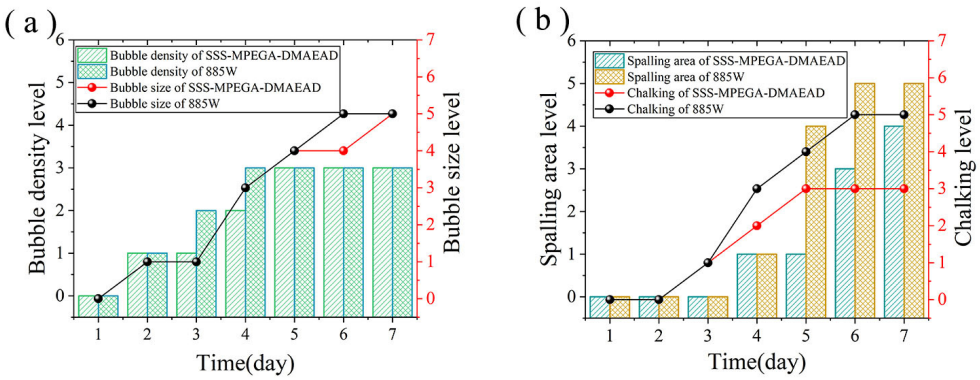

Figure 17. The acid resistance of paint film. (**a**) Blistering of the paint film in acid; (**b**) Flaking of the paint film in acid.

As the paint film is immersed in the acidic solution and the rust spots form through oxidation, the acid will react, inhibiting further rust spot development. Thus, there will be almost no rust spots, only flaking and chalking. Figure 17b shows the flaking and chalking graph of the paint film in 5% sulfuric acid over time, where the bar graph represents the change in the flaking area and the dotted line graph indicates the change in the chalking level. The flaking occurred when the blistering phenomenon reached a certain level in both experimental groups immersed in the acid solution, with the MixSperse 855 W experimental group exhibiting substantially exposed test panels on day 5 due to the flaking of the paint film. Simultaneously, the homemade dispersant group demonstrated a similar situation on day six. The area of peeling that occurred in both experimental groups enlarged with increasing soaking time. Both experimental groups' flaking started to increase after day four, resulting in more serious chalking, and the degree of chalking increased to different degrees with the increase in soaking time. Overall, the homemade hyperdispersant SMD experimental group marginally outperformed the MixSperse 855 W experimental group.

In summary, the homemade hyperdispersant group's paint film acid resistance is slightly superior to that of 855 W. However, additional additives are required to prepare waterborne coatings with superior acid resistance.

3.4.5. Alkali Resistance of Paint Film

Most paints may also be exposed to alkaline environments during actual use, necessitating the consideration of paint film alkali resistance. Table 6 reveals the changes

in the paint film immersed in a 5% sodium hydroxide solution. The alkali resistance of both experimental groups was superior, showing a strong alkali resistance. This may be attributed to the low hydrogen ion content in the alkaline solution, the CO_2 in the air dissolving in water initially reacting with the alkali solution, and the paint film components not reacting with the alkali, resulting in a more stable state.

Table 6. Alkali resistance test of paints.

Test Items	Test Results
Sparkling	No visible changes in the two experimental groups within seven days
Rusting	No visible changes in the two experimental groups within seven days
Flaking	No visible changes in the two experimental groups within seven days
Chalking	Both experimental groups showed a small amount of pigment particles precipitated on the sixth day

3.4.6. SEM Analysis of Paint Film Surface

Figure 18 shows the SEM images of the surface of the $CaCO_3$ paint film. Figure 18A displays the waterborne $CaCO_3$ paint film containing the SSS–MPEGA–DMAEA hyperdispersant, and Figure 18B illustrates the $CaCO_3$ paint film devoid of dispersant. The inorganic pigment particles on the surface of the film with the hyperdispersant were evenly dispersed, and no obvious defects in the film were observed. The electrostatic non-covalent interactions produced by the hyperdispersant augment intermolecular interactions and facilitate CaCO3 dispersion within the coating [28]. Conversely, the paint film lacking dispersant exhibits marked particle agglomeration and uneven dispersion, resulting in numerous cracks. This is because without the addition of a dispersant, the inorganic pigments, such as $CaCO_3$ of the paint film, will produce a large number of agglomerates and cannot be evenly dispersed. A preponderance of agglomerated pigment particles leads to irregular paint coating thickness, and cracking transpires during the curing process.

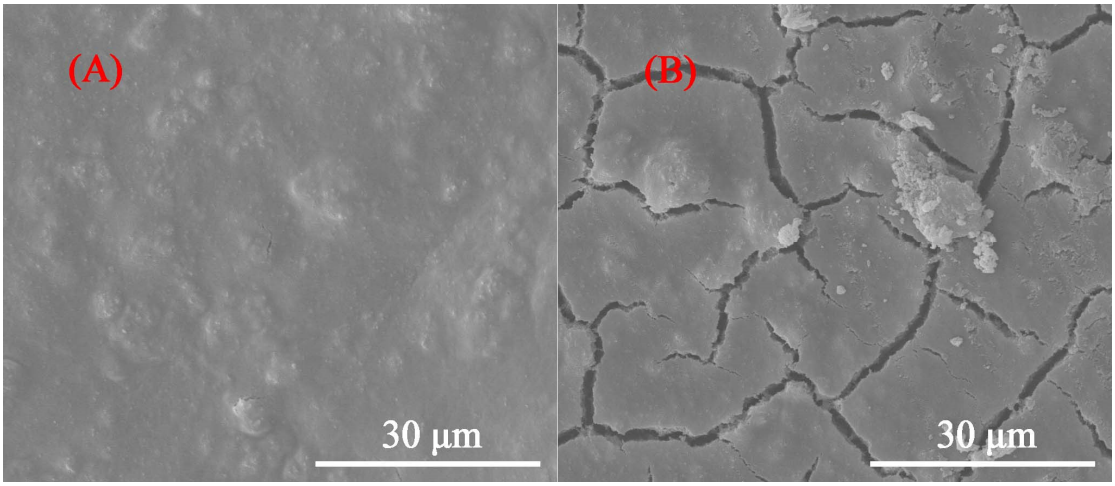

Figure 18. Scanning electron micrograph of the paint film: paint film with dispersant (**A**), paint film without dispersant (**B**).

The $CaCO_3$ coatings with hyperdispersants were immersed in deionized water, 5% H_2SO_4, and 5% NaOH, respectively, and the SEM taken after drying is shown in Figure 19. It is seen from the figure that the $CaCO_3$ coatings in 5% H_2SO_4 and 5% NaOH have different degrees of color change, which means that the coatings are corroded by the solutions. At the same time, the $CaCO_3$ of the three coatings remains evenly distributed, and the part of $CaCO_3$ destroyed is relatively small. This means that the hyperdispersant increases the stability of the coating and makes the $CaCO_3$ less damaged in different environments.

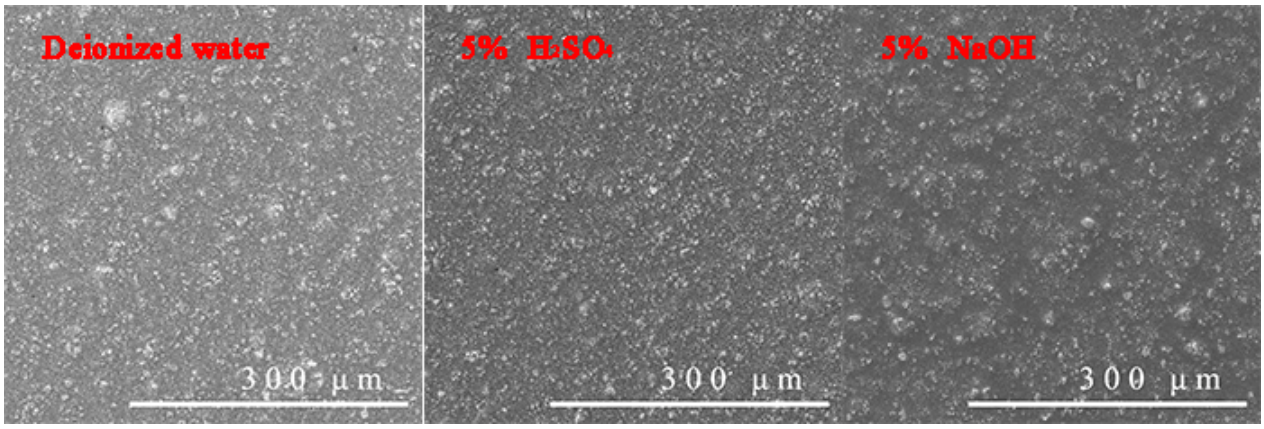

Figure 19. Scanning electron micrograph of $CaCO_3$ coatings infiltrated with different solutions.

4. Conclusions

In this paper, a new hyperdispersant SMD was prepared by aqueous polymerization method using SSS, MPEGA, and DMAEA as monomers. The hyperdispersant generated by this method not only offered the outstanding dispersion of light calcium carbonate but also demonstrated favorable economic efficiency and environmentally friendly attributes, addressing the issues of particle agglomeration and high viscosity in $CaCO_3$ aqueous dispersions. Central composite design optimization yielded an ideal monomer ratio of n(SSS):n(MPEGA):n(DMAEA) = 9:1:5.4. For a 2500-mesh light calcium carbonate slurry with 50% solid content, the optimal hyperdispersant dosage of 0.5% reduced slurry viscosity to 60.3 mPa·s and average particle size to 1071.4 nm. Concurrently, water-based white coatings produced by SMD exhibited excellent storage stability and corrosion resistance, offering promising applications in white coating production.

Author Contributions: Conceptualization, J.B. and Y.L.; methodology, Y.L.; software, Y.L.; validation, J.B.; formal analysis, J.B.; investigation, J.B.; resources, J.B.; data curation, J.B.; writing—original draft preparation, J.B. and Y.L.; writing—review and editing, J.B.; visualization, J.B.; supervision, Y.L.; project administration, J.B. All authors have read and agreed to the published version of the manuscript.

Funding: This research received no external funding and the APC was funded by J.B.

Institutional Review Board Statement: Not applicable.

Informed Consent Statement: Not applicable.

Data Availability Statement: All data that support the findings of this study are included within the article.

Conflicts of Interest: The authors declare no conflict of interest.

References

1. Hong, T.; He, Y.; Xu, Z. Preparation and characterization of calcium carbonate–titanium dioxide core–shell ($CaCO_3$@TiO_2) nanoparticles and application in the papermaking industry. *Powder Technol.* **2015**, *283*, 308–314. [CrossRef]
2. Alali, F.M.; Tarakji, B.; Alqahtani, A.S.; Alqhtani, N.R.; Nabhan, A.B.; Alenzi, A.; Alrafedah, A.; Robaian, A.; Noushad, M.; Kujan, O.; et al. Characterization of superhydrophobic epoxy coatings embedded by modified calcium carbonate nanoparticles. *Prog. Org. Coat.* **2016**, *101*, 577–586. [CrossRef]
3. Ghari, H.S.; Jalali-Arani, A. Nanocomposites based on natural rubber, organoclay and nano-calcium carbonate: Study on the structure, cure behavior, static and dynamic-mechanical properties. *Appl. Clay Sci.* **2016**, *119*, 348–357. [CrossRef]
4. Rudawska, A.; Frigione, M. Cold-Cured Bisphenolic Epoxy Adhesive Filled with Low Amounts of $CaCO_3$: Effect of the Filler on the Durability to Aqueous Environments. *Materials* **2021**, *14*, 1324. [CrossRef]
5. Li, Y.; Gu, W.J.; He, B.G. Investigation into Coating Surface Free Energy and Microstructure of Coated Paper Related to Pigment. In *Advanced Materials Research*; Trans Tech Publications Ltd.: Stafa-Zurich, Switzerland, 2014; Volume 884, pp. 212–215. [CrossRef]
6. Wang, J.; Feng, Y.; Xie, J.; Li, G.; Li, X. Dispersion of phthalocyanine green G in nonaqueous medium using hyperdispersants and application in E-ink. *J. Dispers. Sci. Technol.* **2006**, *27*, 975–981. [CrossRef]

7. Farrokhpay, S. A review of polymeric dispersant stabilisation of titania pigment. *Adv. Colloid Interface Sci.* **2009**, *151*, 24–32. [CrossRef] [PubMed]
8. Sis, H.; Birinci, M. Wetting and rheological characteristics of hydrophobic organic pigments in water in the presence of non-ionic surfactants. *Colloids Surf. A Physicochem. Eng. Asp.* **2014**, *455*, 58–66. [CrossRef]
9. Liu, W.; Cheng, L.; Yao, X.; Fang, R.; Liu, G. Synthesis and properties of novel acrylic polyester hyper-dispersant. *J. Coat. Technol. Res.* **2016**, *13*, 763–768. [CrossRef]
10. Bayer, I.S. Superhydrophobic coatings from ecofriendly materials and processes: A review. *Adv. Mater. Interfaces* **2020**, *7*, 2000095. [CrossRef]
11. Barrino, F.; De La Rosa-Ramírez, H.; Schiraldi, C.; López-Martínez, J.; Samper, M.D. Preparation and Characterization of New Bioplastics Based on Polybutylene Succinate (PBS). *Polymers* **2023**, *15*, 1212. [CrossRef]
12. Qian, T.; Zhong, Y.; Mao, Z.; Xu, H.; Zhang, L.; Sui, X.; Wang, B. The comb-like modified styrene-maleic anhydride copolymer dispersant for disperse dyes. *J. Appl. Polym. Sci.* **2019**, *136*, 47330. [CrossRef]
13. Xu, Y.; Liu, J.; Du, C.; Fu, S.; Liu, X. Preparation of nanoscale carbon black dispersion using hyper-branched poly (styrene-alt-maleic anhydride). *Prog. Org. Coat.* **2012**, *75*, 537–542. [CrossRef]
14. Tian, Q.; Zhang, Q. Synthesis and performance of sodium salt of MAA/St/SAS copolymer dispersant. *IOP Conf. Ser. Earth Environ. Sci. IOP Publ.* **2019**, *310*, 042032. [CrossRef]
15. Zhang, G.; Zhu, N.; Zhu, X. Influence of Polycarboxylate Dispersants with Different Molecular Structures on the Performance of Coal Water Slurry. *J. Dispers. Sci. Technol.* **2016**, *37*, 1799–1805. [CrossRef]
16. Du, L.; Zhang, G.; Yang, D.; Luo, J.; Liu, Y.; Zhang, W.; Zhang, C.; Li, J.; Zhu, J. Synthesis of a novel amphoteric copolymer and its application as a dispersant for coal water slurry preparation. *R. Soc. Open Sci.* **2021**, *8*, 201480. [CrossRef]
17. Lu, X.; Xia, Y.; Liu, M.; Qian, Y.; Zhou, X.; Gu, N. Improved performance of diatomite-based dental nanocomposite ceramics using layer-by-layer assembly. *Int. J. Nanomed.* **2012**, *7*, 2153. [CrossRef]
18. Obata, M.; Tanaka, S.; Mizukoshi, H.; Ishihara, E.; Takahashi, M.; Hirohara, S. RAFT synthesis of polystyrene-block-poly (polyethylene glycol monomethyl ether acrylate) for zinc phthalocyanine-loaded polymeric micelles as photodynamic therapy photosensitizers. *J. Polym. Sci. Part A Polym. Chem.* **2018**, *56*, 560–570. [CrossRef]
19. Touaiti, F.; Alam, P.; Nilsson, R.; Pahlevan, M.; Ansell, M.; Wilen, C.; Toivakka, M. Thermomechanical properties of $CaCO_3$-latex pigment coatings: Impact of modified dispersing agents. *Prog. Org. Coat.* **2013**, *76*, 439–446. [CrossRef]
20. Büyükyağcı, A.; Tuzcu, G.; Aras, L. Synthesis of copolymers of methoxy polyethylene glycol acrylate and 2-acrylamido-2-methyl-1-propanesulfonic acid: Its characterization and application as superplasticizer in concrete. *Cem. Concr. Res.* **2009**, *39*, 629–635. [CrossRef]
21. Liu, J.; Li, J.; Wang, C.Y.; Ren, Q. RAFT surfactant-free cationic emulsion polymerization of styrene: Effect of hydrophobicity of block macro-RAFT agent. *J. Macromol. Sci. Part A* **2020**, *58*, 232–242. [CrossRef]
22. Liu, S.H.; Wu, T.; Lu, Y.M.; Li, H.-S. Particular thermal behavior of 2, 2′-azobis [2-(2-imidazolin-2-yl) propane] dihydrochloride using DSC and STA. *J. Therm. Anal. Calorim.* **2021**, *144*, 343–349. [CrossRef]
23. Ferreira SL, C.; Lemos, V.A.; de Carvalho, V.S.; da Silva, E.G.; Queiroz, A.F.; Felix, C.S.; da Silva, D.L.; Dourado, G.B.; Oliveira, R.V. Multivariate optimization techniques in analytical chemistry-an overview. *Microchem. J.* **2018**, *140*, 176–182. [CrossRef]
24. Song, J.O.; McCormick, A.V.; Francis, L.F. Depthwise Viscosity Gradients in UV-Cured Epoxy Coatings. *Macromol. Mater. Eng.* **2013**, *298*, 145–152. [CrossRef]
25. Khan, M.; Hamid, A.; Tiehu, L.; Zada, A.; Attique, F.; Ahmad, N.; Ullah, A.; Hayat, A.; Mahmood, I.; Hussain, A.; et al. Surface optimization of detonation nanodiamonds for the enhanced mechanical properties of polymer/nanodiamond composites. *Diam. Relat. Mater.* **2020**, *107*, 107897. [CrossRef]
26. Chakraborty, S.; Sarkar, I.; Behera, D.K.; Pal, S.K.; Chakraborty, S. Experimental investigation on the effect of dispersant addition on thermal and rheological characteristics of TiO_2 nanofluid. *Powder Technol.* **2017**, *307*, 10–24. [CrossRef]
27. Khan, M.; Tiehu, L.; Hussain, A.; Raza, A.; Zada, A.; Alei, D.; Khan, A.R.; Ali, R.; Hussain, H.; Hussain, J.; et al. Physiochemical evaluations, mechanical attenuations and thermal stability of graphene nanosheets and functionalized nanodiamonds loaded pitch derived carbon foam composites. *Diam. Relat. Mater.* **2022**, *126*, 109077. [CrossRef]
28. Sethi, S.K.; Manik, G. A combined theoretical and experimental investigation on the wettability of MWCNT filled PVAc-g-PDMS easy-clean coating. *Prog. Org. Coat.* **2021**, *151*, 106092. [CrossRef]